Acoustic full-waveform inversion in an elastic world

Oscar Calderon Agudo, Nuno Vieira da Silva, Michael Warner and Joanna Morgan, Imperial College London*

Summary

Despite the elastic nature of the earth, wave propagation in the subsurface is normally modeled using the acoustic anisotropic wave equation, in part due to the requirement to be efficient when dealing with large 3D datasets. This simplification has a negative effect on the quality of recovered P-wave models, as it means that amplitude information in the observed data cannot be fully utilized when applying full-waveform inversion (FWI) (Warner et al., 2013). We examine the consequences of using an acoustic wave propagator in two synthetic examples, and we propose a method to mitigate elastic effects in acoustic FWI based on matching filters. We find that our proposed approach is successful: the recovered P-wave models are better resolved than those obtained using conventional acoustic FWI.

Introduction

Full-waveform inversion (FWI) is used to build models of the subsurface by minimizing the misfit between observed and modeled data (Tarantola, 1986). To invert 3D datasets efficiently, seismic wave propagation is normally modeled with the acoustic anisotropic wave equation. This approach accounts for the correct kinematics of the acoustic wavefield, but it does not consider phase conversions of the wavefield at interfaces (P- to S-wave conversions in an isotropic earth), which affect the amplitude of all arrivals, including the first-arriving P-waves (Hobro et al., 2014).

To obtain more reliable properties of the subsurface we must address the dynamics of the recorded wavefield (Warner et al., 2012), which means that elastic effects must be accounted for. Elastic FWI is, however, not yet widely used due to: 1) the high computational cost of elastic modeling; 2) the non-unique and coupled effect of the different physical properties on the seismic wavefield; and 3) the inherent difficulty in modeling amplitudes produced by inaccuracies in the source wavelet, and often poorly-known parameters such as subsurface density, attenuation and S-wave velocity.

Chapman et al. (2010) recently suggested a method to address elastic amplitude effects at interfaces by adding a correction term to the acoustic wave equation. Although this scheme would increase the computational cost of acoustic FWI by a factor of ~ 2, it has the potential to allow better utilization of amplitude information and consequent improvement of the recovered P-wave models (Veitch et al., 2012).

In this paper we propose and implement an alternative strategy to address a wider range of elastic effects in acoustic FWI through the use of matching filters.

Method

To address elastic effects in acoustic inversion of elastic data we propose the following workflow:

1. Perform acoustic inversion of the observed (elastic) data to recover a P-wave velocity model.
2. Generate acoustic and elastic data using the recovered P-wave model and an estimated model of v_p/v_s.
3. Determine matching filters that match the predicted elastic data to the predicted acoustic data obtained in step 2.
4. Apply the matching filters to the observed data to reduce elastic effects.
5. Perform acoustic inversion of the matched observed data.

The workflow can be applied in an iterative fashion to further mitigate elastic effects, i.e. by re-starting the flow from the second step. In terms of computational resources, the workflow requires forward modeling of acoustic and elastic data and an additional acoustic inversion step. Thus, the method is two to three times more demanding than acoustic FWI but is still an order of magnitude less demanding than elastic FWI (Guasch et al., 2010).

Overthrust land model

We first test our approach using the 2D SEG/EAGE overthrust P-wave velocity model, but remove the water layer so that it is effectively a land model (Figure 1). This is a better test of our scheme, as it leads to the generation of a synthetic seismic dataset with a stronger elastic component. We design an S-wave velocity model assuming a constant Poisson's ratio of 0.24 (Brossier et al., 2009), i.e. a constant velocity ratio of $v_p/v_s \approx 1.77$. We use a grid spacing of 10 m to ensure that there is no dispersion of either P- or S-waves below 17.5 Hz. We generate both

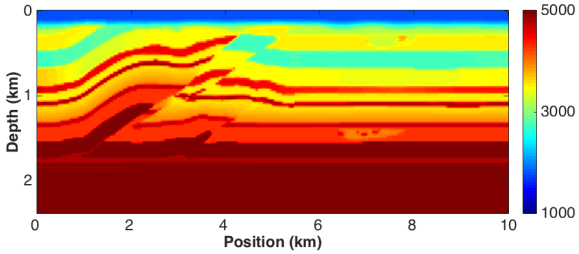

Figure 1: Overthrust P-wave land model.

acoustic and elastic single-component pressure data from these velocity models using a single line of 95 sources at 5 m depth and a dense array of 961 receivers at 15 m depth that cover the entire model. We use a source wavelet with a useful bandwidth that spans from 2 Hz up to 17 Hz, and absorbing boundaries to mitigate spurious reflections at the model edges. Consequently, as would be expected for a land field dataset, shear waves are generated near the sources given that they are located in a layer with non-zero S-wave velocities.

Figures 2a and 2b show the modeled acoustic and elastic data for a representative shot gather at the center of the model generated using the true P- and S-wave velocity models. Figure 2e shows the difference between the elastic and acoustic data. Additionally, we observe events in Figure 2b corresponding to both S-waves and converted P- to S-waves that are not present in the true acoustic data (e.g. refractions with a different slope not visible in the true acoustic data).

Figure 3 illustrates the relative improvement in recovered v_p when using our proposed workflow. Figure 3a is the starting P-wave velocity model, obtained after smoothing the true P-wave velocity model (in slowness) 180 times with a Gaussian function of 30 m correlation length. Figure 3b shows the recovered model when applying acoustic FWI to acoustic data: this is considered to be the ideal solution – should we be able to remove all elastic effects from the data. The different layers of the true P-wave velocity model are well recovered when data are inverted within the bandwidth 3.5 Hz to 16.7 Hz, with a total of 144 iterations. Figure 3c shows the result of inverting elastic data with acoustic FWI – which represents the normal situation when inverting real field data. This leads to a recovered P-wave velocity model with poorer resolution in which the layers are not so well defined. We also observe in Figure 3c that, due to the slow S-wave velocities at the top of the model, the low velocity channel at about 800 m depth on the right-hand-side of the thrust is incorrectly pushed down when applying an acoustic inversion to elastic data.

In step 2 of our approach, predicted acoustic and elastic data are generated using the recovered P-wave velocity model (Figure 3c) and an S-wave velocity model built using $v_p/v_s \approx 1.77$. A matching filter that matches the elastic to the acoustic modeled data is then computed (Step 3) and it is convolved with the true elastic data (Step 4) to remove elastic effects from the data (e.g. Figure 2c). The matched elastic data is then inverted acoustically (Step 5)

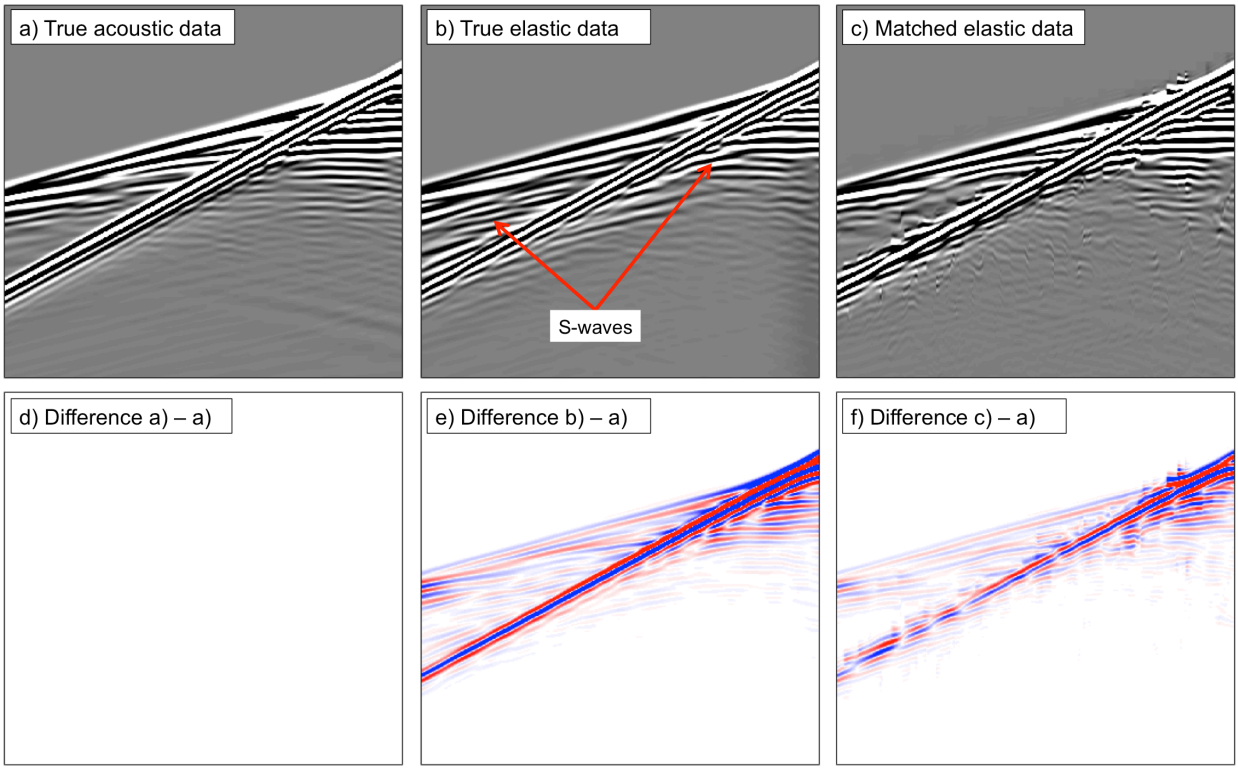

Figure 2: Traces of a representative shot gather of a) the true acoustic data, b) the true elastic data and c) the matched elastic data for a shot at the centre of the overthrust land model. The bottom panels show the difference of each of the panels above with the true acoustic data in panel a).

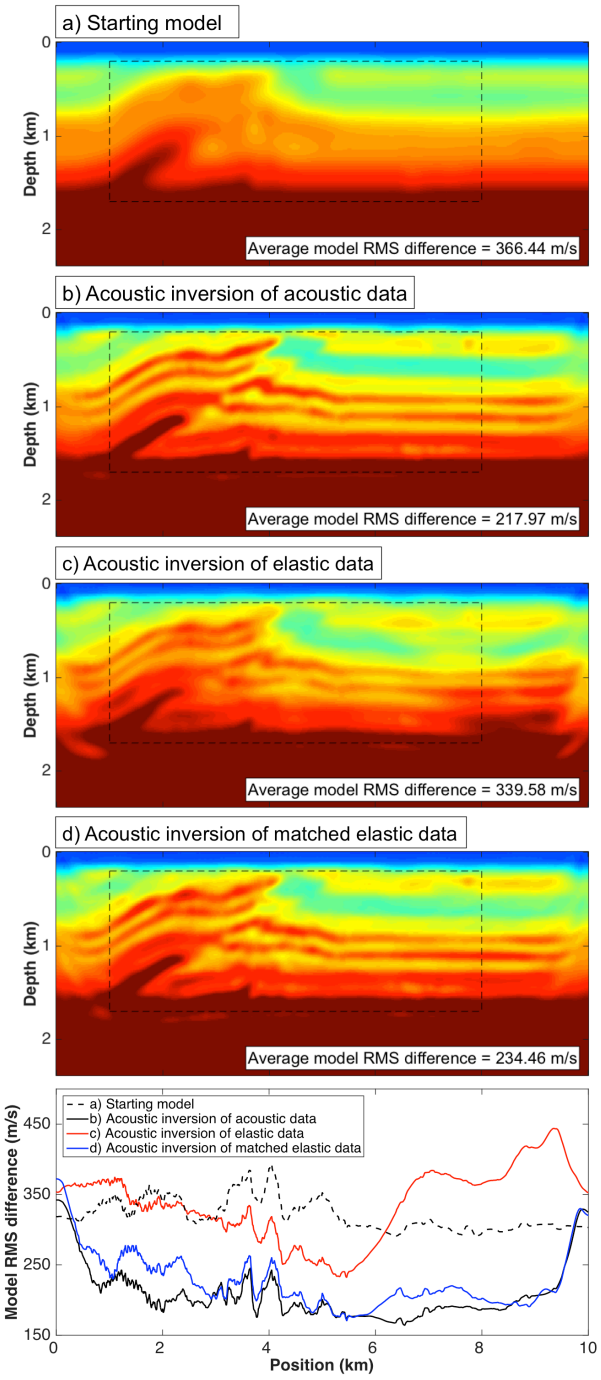

Figure 3: Vertical slices of a) the starting P-wave model and the FWI-recovered P-wave models after acoustic inversion of b) true acoustic data, c) true elastic data and d) matched elastic data. The bottom panel shows the model RMS difference as a function of position for the panels above.

and the workflow can be applied again to further mitigate elastic effects if required. The difference between the true (Figure 2a) and matched data (Figure 2c) is shown in Figure 2f. The reduced amplitudes of all arrivals in comparison to Figure 2e, demonstrates that the elastic effects have been partially removed by the matching filter. We note, however, the presence of small artefacts in the matched data in Figure 2c that are due to the fact that we are matching two datasets with different spectra. We have minimized their impact by matching the data in a trace-by-trace approach using short filters and appropriately weighting and stacking the matched data along each trace.

The result of inverting the matched elastic data with acoustic FWI is shown in Figure 3d. The resulting P-wave velocity model is much better resolved (as indicated by the RMS values on the figure): the different layers can be clearly differentiated and the low-velocity channel at the top of the model is in its correct position.

To further assess the quality of the inverted models, the RMS difference with respect to the true velocity model as a function of position is plotted at the bottom panel of Figure 3. The smaller this value, then the closer the model is to the true model. We observe the benefit of using the current method to mitigate elastic effects, as the recovered P-wave model after acoustic FWI of the matched elastic data (blue line) is closer to the true model for most positions when compared to the model after acoustic FWI of elastic data (red line). As expected, the result of the data matching workflow does not result in a model better than the result of acoustic FWI of acoustic data (black line), and is much better than the starting model (dotted line).

Figure 4 shows the RMS misfit per iteration for the different inversions. We make three observations: 1) the average model RMS difference decreases with increasing frequencies (i.e. more iterations); 2) this decrease is not so pronounced for the acoustic inversion of elastic and matched elastic data; and 3) after mitigating elastic effects, the average model RMS difference per iteration is reduced (blue curve) and is closer to the variation of the difference after acoustic inversion of acoustic data. Thus, the present workflow has strongly mitigated elastic effects, providing a significantly improved P-wave velocity model of the subsurface.

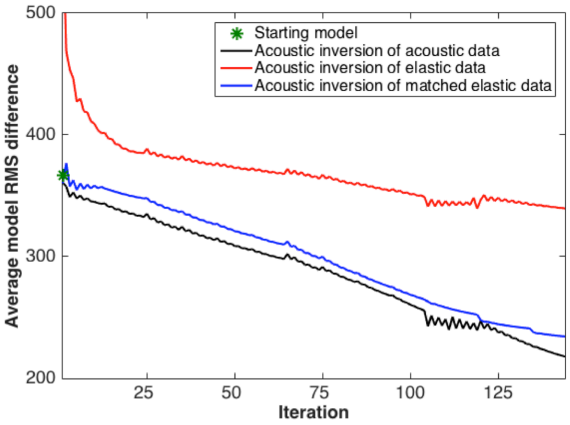

Figure 4: Average model RMS difference of the starting and FWI-recovered P-wave models in Figure 3 computed inside the dotted box area as a function of iteration.

Chevron SEG 2014 synthetic blind dataset

Next we apply the same methodology to the Chevron SEG 2014 synthetic blind dataset. This synthetic dataset was generated using a realistic visco-elastic isotropic subsurface model based on field seismic data and rock physics data, in which the density and velocity do not follow a known relationship. Ambient noise, surface ghosts and multiples are present in the data. There are a total of 1600 shots and 321 receivers per shot, with a maximum offset of 8 km. In the examples shown here, we used a grid spacing of 12.5 m, performed acoustic FWI for frequencies between 4.5 Hz and 23.5 Hz for the whole model, and display the uppermost 2 km of the resulting models where turning-ray coverage is good. The starting model is shown in Figure 5a, and the result of acoustic FWI of the observed data is shown in Figure 5b (Step 1 of our proposed workflow).

Unlike the previous synthetic result, here we do not know the true S-wave velocity model. We proceed by making what we expect to be a realistic estimation of the v_p/v_s ratio and apply the remaining steps of the workflow to recover the P-wave velocity model shown in Figure 5c. When compared to Figure 5b, we observe an improved overall resolution of the layers: note the sharpness and continuity of the intermediate velocity channels at 1.2 – 1.5 km depth.

Discussion

The next step of our research will focus on assessing the impact of using an incorrect estimated model of v_p/v_s. However, the success of the application of our workflow to the Chevron SEG 2014 synthetic blind dataset, as well as other tests not shown here, suggest that a smooth v_p/v_s estimation not far from the true ratio at the sea-bottom is enough to mitigate most of the elastic effects in marine datasets. Future work will focus on testing other types of data-matching filters, exploring different regularizations, as well as investigating similar methodologies to compensate for other amplitude effects that are typically not fully accounted for in acoustic FWI.

Conclusions

We have presented and applied a method to mitigate elastic effects in acoustic FWI of elastic data, which is two to three times more demanding than acoustic FWI but much less so than elastic FWI. The successful application of our proposed scheme to a synthetic land and realistic marine dataset shows that it has the potential to improve the recovery of P-wave velocity from field data, without having to use an elastic wave-field propagator.

Acknowledgments

We would like to thank Chevron for preparing the synthetic blind dataset.

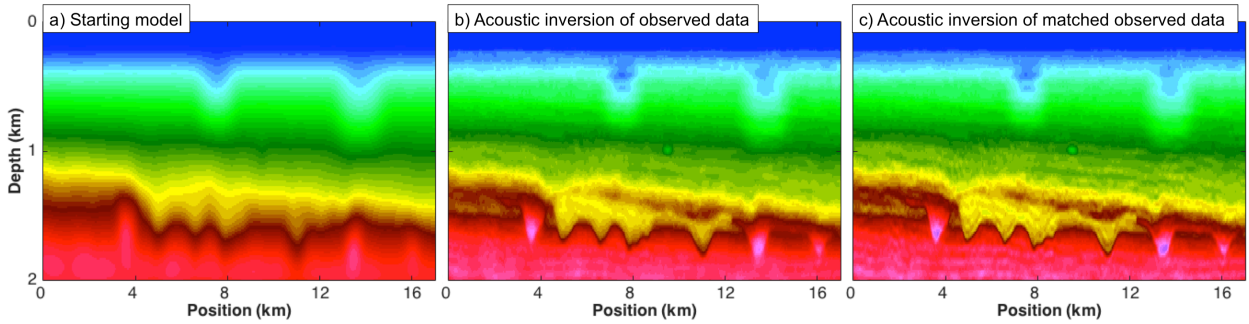

Figure 5: Vertical slices of the first 2 km through the a) starting P-wave model and the FWI-recovered P-wave models after b) acoustic inversion of the observed data and c) acoustic inversion of matched observed data for the SEG 2014 synthetic blind dataset.

EDITED REFERENCES

Note: This reference list is a copyedited version of the reference list submitted by the author. Reference lists for the 2016 SEG Technical Program Expanded Abstracts have been copyedited so that references provided with the online metadata for each paper will achieve a high degree of linking to cited sources that appear on the Web.

REFERENCES

Brossier, R., S. Operto, and J. Virieux, 2009, Seismic imaging of complex onshore structures by 2D elastic frequency-domain full-waveform inversion: Geophysics, **74**, WCC105–WCC118, http://dx.doi.org/10.1190/1.3215771.

Chapman, C. H., J. Hobro, and J. O. A. Robertsson, 2010, Elastic corrections to acoustic finite-difference simulations: 73rd Annual International Conference and Exhibition, EAGE, Extended Abstracts, **29**, 3013–3017, http://dx.doi.org/10.3997/2214-4609.20148955.

Guasch, L., M. Warner, I. Stekl, and A. Umpleby, 2010, 3D Elastic wavefield inversion in the time domain: 72nd Annual International Conference and Exhibition, EAGE, Extended Abstracts.

Hobro, J. W. D., C. H. Chapman, and J. O. A. Robertsson, 2014, A method for correcting acoustic finite-difference amplitudes for elastic effects: Geophysics, **79**, no. 4, T243–T255, http://dx.doi.org/10.1190/geo2013-0335.1.

Tarantola, A., 1986, A strategy for nonlinear elastic inversion of seismic reflection data: Geophysics, **51**, 1893–1903, http://dx.doi.org/10.1190/1.1442046.

Veitch, B., J. Rickett, and J. Hobro, 2012, Imaging elastic media by corrections to acoustic propagation: 82nd Annual International Meeting, SEG, Expanded Abstracts, 1–5.

Warner, M., J. Morgan, A. Umpleby, I. Stekl, and L. Guasch, 2012, Which physics for full-wavefield seismic inversion? 74th Annual International Conference and Exhibition, EAGE, Extended Abstracts, 4–7.